Supporting Information for "MJO Initiation Triggered by the Amplification of Upper-tropospheric Dry Mixed Rossby–gravity Waves"

Daisuke Takasuka[1], Tsubasa Kohyama[2], Hiroaki Miura[3], and Tamaki Suematsu[4]

[1]Japan Agency for Marine-Earth Science and Technology, Yokohama, Japan

[2]Department of Information Sciences, Ochanomizu University, Tokyo, Japan

[3]Department of Earth and Planetary Sciences, The University of Tokyo, Tokyo, Japan

[4]Atmosphere and Ocean Research Institute, The University of Tokyo, Kashiwa, Japan

Contents of this file

Introduction

Text S1 provides derivation of the simple dry model used in the main text (Equations (1)–(4)). In Text S2, we show the formulation of the time-invariant heat sources and initial MRG structure given to the model. Text S3 explains the methodology of ray tracing of MRGs. Figure S1 presents the relationship between low-level MRG convergence and MJO2 initiation in the Indian Ocean, and Figures S2–S4 supplementarily display the structure and evolution of MRGs for the model and MJO2.

Text S1. Detailed derivation of the simple dry model

We here derive the simple dry model utilized in the main text, which starts with the three-dimensional Boussinesq system on the equatorial β-plane (Majda, 2003):

$$\frac{D\mathbf{U}}{Dt} + \beta y \mathbf{U}^{\perp} = -\nabla P + \hat{S}_{\mathbf{U}} \tag{1}$$

$$\nabla \cdot \mathbf{U} + \frac{\partial W}{\partial z} = 0 \tag{2}$$

$$\frac{\partial P}{\partial z} = g\frac{\Theta}{\theta_{\mathrm{ref}}} \tag{3}$$

$$\frac{D\Theta}{Dt} + W\frac{d\overline{\theta}}{dz} = \hat{S}_{\theta} \tag{4}$$

where $\mathbf{U} = (U(x,y,z,t), V(x,y,z,t))^T$ is the horizontal wind vector; $\mathbf{U}^{\perp} = (-V, U)^T$; W is vertical velocity; P is pressure including density; Θ is potential temperature anomalies from the basic state ($= \theta_{\mathrm{ref}} + \overline{\theta}(z)$ where θ_{ref} is constant); g is gravitational acceleration; and $\hat{S}_{\theta}$ and $\hat{S}_{\mathbf{u}}$ is the heat and momentum source, respectively. ∇ is the horizontal gradient operator $(\partial/\partial x, \partial/\partial y)$, and the material derivative (D/Dt) is

$$\frac{D}{Dt} = \frac{\partial}{\partial t} + \mathbf{U} \cdot \nabla + W\frac{\partial}{\partial z}$$

Equations (1)–(4) with dimensions are then nondimensionalized by the scaling introduced in Stechmann, Majda, and Khouider (2008), which leads to the following equations:

$$\frac{D\mathbf{U}}{Dt} + y \mathbf{U}^{\perp} = -\nabla P + \hat{S}_{\mathbf{U}} \tag{5}$$

$$\nabla \cdot \mathbf{U} + \frac{\partial W}{\partial z} = 0 \tag{6}$$

$$\frac{\partial P}{\partial z} = \Theta \tag{7}$$

$$\frac{D\Theta}{Dt} + W = \hat{S}_{\theta} \tag{8}$$

where all variables, forcing, and operators in (5)–(8) have no dimensions.

Imposing the rigid lid conditions at the surface and at the top of the troposphere (i.e., $W = 0$ at $z = 0,\ H$; in nondimensional units, $z = 0,\ \pi$), we expand the variables and sources in (5)–(8) in terms of the vertical eigenmodes (C_j, S_j) as follows:

$$\begin{aligned}
\mathbf{U}(x,y,z,t) &= \sum_{j=0}^{\infty} \mathbf{u}_j(x,y,t)C_j(z), \quad W(x,y,z,t) = \sum_{j=0}^{\infty} w_j(x,y,t)S_j(z) \\
P(x,y,z,t) &= \sum_{j=0}^{\infty} p_j(x,y,t)C_j(z), \quad \Theta(x,y,z,t) = \sum_{j=0}^{\infty} \theta_j(x,y,t)jS_j(z) \\
\hat{S}_{\mathbf{U}}(x,y,z,t) &= \sum_{j=0}^{\infty} S_{\mathbf{u}_j}(x,y,t)C_j(z), \quad \hat{S}_{\theta}(x,y,z,t) = \sum_{j=0}^{\infty} S_{\theta_j}(x,y,t)S_j(z)
\end{aligned} \tag{9}$$

where the vertical modes C_j, S_j are defined as

$$C_0 = 1, \quad C_j = \sqrt{2}\cos(jz), \quad S_j = \sqrt{2}\sin(jz) \quad (j = 1, 2, 3...)$$

and for those eigenfunctions, the inner product is defined as

$$\langle F(z), G(z)\rangle = \frac{1}{\pi}\int_0^{\pi} F(z)G(z)dz$$

For a set of equations (9), we assume that the variables and sources are decomposed by the barotropic mode ($j = 0$) and/or first and second baroclinic modes ($j = 1, 2$), because they can capture the main structure of equatorial waves (e.g., Takayabu et al., 1996; Haertel & Kiladis, 2004; Kiladis et al., 2009). That is,

$$\begin{aligned}
\mathbf{U} &= \mathbf{u}_0 + C_1\mathbf{u}_1 + C_2\mathbf{u}_2, \qquad W = w_0 + S_1w_1 + S_2w_2 \\
P &= p_0 + C_1p_1 + C_2p_2, \qquad \Theta = S_1\theta_1 + 2S_2\theta_2 \\
\hat{S}_{\mathbf{u}} &= S_{\mathbf{u}_0} + C_1S_{\mathbf{u}_1} + C_2S_{\mathbf{u}_2}, \quad \hat{S}_{\theta} = S_1S_{\theta_1} + S_2S_{\theta_2}
\end{aligned} \tag{10}$$

Here, the vertical modes for W are restricted by the following arguments. If we substitute the decomposed $\mathbf{U}$ and W into the continuity equation (6) and then compute the inner

product with C_0, we obtain

$$\nabla \cdot \mathbf{u}_0 + \frac{\partial w_0}{\partial z} = 0 \tag{11}$$

Integration of (11) from $z' = 0$ to $z' = z$ derives

$$\int_0^z (\nabla \cdot \mathbf{u}_0) dz' + w_0(z) - w_0(0) = 0,$$

so using $w_0(z' = 0) = 0$, we can rewrite this as $w_0(z) = -z(\nabla \cdot \mathbf{u}_0)$. Because the boundary condition $w_0(\pi) = 0$ should be satisfied, $\nabla \cdot \mathbf{u}_0 = 0$ is necessary. Hence, the barotropic mode for W must vanish:

$$w_0 = 0 \tag{12}$$

Under the vertical decomposition in (10) and (12), equations (5)–(8) are projected onto the barotropic and/or first and second baroclinic modes. As an example, we now derive the momentum equation with the barotropic mode. Substitution of (9) into (5) leads to

$$\frac{\partial}{\partial t}\left(\sum_{j=0}^{2} C_j \mathbf{u}_j\right) + \sum_{j=0}^{2} C_j \mathbf{u}_j \cdot \nabla \left(\sum_{j=0}^{2} C_j \mathbf{u}_j\right) + \left(\sum_{j=1}^{2} S_j w_j\right) \frac{\partial}{\partial z}\left(\sum_{j=1}^{2} C_j \mathbf{u}_j\right) + y\left(\sum_{j=0}^{2} C_j \mathbf{u}_j^{\perp}\right) = C_1 \nabla\theta_1 + C_2 \nabla\theta_2 + \sum_{j=0}^{2} C_j S_{\mathbf{u}_j} \tag{13}$$

where $P_j = -\theta_j$ from the hydrostatic equation (7) is used. To extract the barotropic mode from (13), we compute the inner product between (13) and C_0, which derives

$$\frac{\partial \mathbf{u}_0}{\partial t} + \sum_{j=0}^{2} \mathbf{u}_j \cdot \nabla \mathbf{u}_j - \sum_{j=1}^{2} w_j \mathbf{u}_j + y\mathbf{u}_0^{\perp} = S_{\mathbf{u}_0} \tag{14}$$

By applying $w_j = -(1/j)\nabla \cdot \mathbf{u}_j$ from the continuity equation (6) and operating "$\nabla\times$" to (14), we finally obtain the barotropic vorticity (ζ_0) equation:

$$\frac{\partial \zeta_0}{\partial t} + \nabla \times \left[\sum_{j=0}^{2} \mathbf{u}_j \cdot \nabla \mathbf{u}_j + \sum_{j=1}^{2} (\nabla \cdot \mathbf{u}_j)\mathbf{u}_j\right] + v_0 = S_{\zeta_0} \tag{15}$$

where $\zeta_0 = \nabla \times \mathbf{u}_0$, and S_{ζ_0} is the source term for barotropic vorticity. When we adopt $S_{\zeta_0} = -\zeta_0/\tau_{\mathbf{u}}$ and add the diffusion term, the equation (15) corresponds to the equation (1) in the main text. Note that (15) (or (1) in the main text) is numerically solved by predicting a stream function ψ_0, which satisfies the Laplace equation $\zeta_0 = \nabla^2\psi_0$. Following the same procedure as above, we can construct the dry dynamical core completely with equations (1)–(4) in the main text.

Text S2. Description of the heat sources and initial MRG structure for the model

1) Formulations of the time-invariant heat sources

The time-invariant heat sources for the first and second baroclinic modes (S_{θ_1} and S_{θ_2}) are given by

$$S_{\theta_1} = \begin{cases} Q^1_{\theta_1} \cos\left(2\pi \dfrac{x - L_x/16}{L_x/8}\right) \exp(-\beta y^2/c) & \left(0 \le \dfrac{x}{L_x} \le \dfrac{1}{8}\right) \\ (Q^2_{\theta_1} - Q^1_{\theta_1}) + Q^2_{\theta_1} \cos\left[2\pi \dfrac{x - (19/48)L_x}{(13/24)L_x}\right] \exp(-\beta y^2/c) & \left(\dfrac{1}{8} < \dfrac{x}{L_x} < \dfrac{2}{3}\right) \\ (Q^3_{\theta_1} - Q^1_{\theta_1}) + Q^3_{\theta_1} \cos\left[2\pi \dfrac{x - (5/6)L_x}{L_x/3}\right] \exp(-\beta y^2/c) & \left(\dfrac{2}{3} \le \dfrac{x}{L_x} \le 1\right) \end{cases} \quad (16)$$

$$S_{\theta_2} = \begin{cases} Q_{\theta_2} \left|\cos\left(2\pi \dfrac{x - L_x/16}{L_x/8}\right)\right| \exp(-\beta y^2/c) & \left(0 \le \dfrac{x}{L_x} \le \dfrac{1}{8}\right) \\ Q_{\theta_2} \left|\cos\left[2\pi \dfrac{x - (19/48)L_x}{(13/24)L_x}\right]\right| \exp(-\beta y^2/c) & \left(\dfrac{1}{8} < \dfrac{x}{L_x} < \dfrac{2}{3}\right) \\ Q_{\theta_2} \left|\cos\left[2\pi \dfrac{x - (5/6)L_x}{L_x/3}\right]\right| \exp(-\beta y^2/c) & \left(\dfrac{2}{3} \le \dfrac{x}{L_x} \le 1\right) \end{cases} \quad (17)$$

where L_x (= 40,000 km) is the zonal extent of the channel and c (= 50 m/s) is the reference phase speed of gravity waves (Stechmann et al., 2008). Heating amplitudes are

set at $(Q^1_{\theta_1},\ Q^2_{\theta_1},\ Q^3_{\theta_1}) = (1.0,\ 1.5,\ 0.75)$ K/day, and $Q_{\theta_2} = 0.226$ K/day. As described in the main text, Q_{θ_2} is the same as that in Yang, Khouider, Majda, and Chevrotière (2019).

2) Formulations of the initial MRG structure

Following Aiyyer and Molinari (2003), we construct the initial MRG structure on the equatorial β-plane. For the first and second baroclinic modes ($j = 1,\ 2$), u_j, v_j, and θ_j associated with MRGs at $t = 0$ are given by

$$v_j|_{t=0} = A_j \phi e^{-\beta y^2/2c} \cos(kx) \tag{18}$$

$$u_j|_{t=0} = A_j \beta y \frac{e^{-\beta y^2/2c}}{k^2c^2 - \omega^2}[(\omega + ck)\phi + 2ck\gamma\phi^*] \sin(kx) \tag{19}$$

$$\theta_j|_{t=0} = -A_j \beta y \overline{\alpha} \frac{e^{-\beta y^2/2c}}{c(k^2c^2 - \omega^2)}[(\omega + ck)\phi + 2\omega\gamma\phi^*] \sin(kx) \tag{20}$$

Here, A_j is an arbitrary amplitude factor; k is zonal wavenumber; ω is frequency; $\overline{\alpha} \equiv HN^2\theta_{\rm ref}/(\pi g)$ is potential temperature scale (N^2 is buoyancy frequency squared; see Stechmann et al. (2008)); and $(\phi, \phi^*; \gamma)$ satisfies the following relation:

$$\phi = {}_1F_1\left(-\frac{\gamma}{2}, \frac{1}{2}, \frac{\beta y^2}{c}\right), \quad \phi^* = {}_1F_1\left(1 - \frac{\gamma}{2}, \frac{3}{2}, \frac{\beta y^2}{c}\right) \tag{21}$$

$$\gamma = \frac{\omega^3 - c^2k\beta - c^2k^2\omega - \beta c\omega}{2\beta c\omega} \tag{22}$$

where ${}_1F_1$ is a Kummer's confluent hypergeometric function. Because $v_j|_{t=0}$ should be vanished at the meridional boundary $y = \pm L_y$ in the equatorial β-channel,

$${}_1F_1\left(-\frac{\gamma}{2}, \frac{1}{2}, \frac{\beta {L_y}^2}{c}\right) = 0 \tag{23}$$

is required from (18) and (21). γ can be numerically obtained from (23), and then a solution of ω in (22) can also be found for given k. As the result, we know all parameters needed to derive the MRG structure from (18)–(20). In this study, the MRG horizontal and vertical structure for $A_1 = -3.0$ and $A_2 = 3.0$ is used, and it is presented in Fig. S2.

Text S3. Method of ray tracing for MRGs (Fig. 4h)

We have conducted ray tracing for MRGs in an equatorial x-z space by integrating the group velocity $\mathbf{C}_g = (C_{gx}, C_{gz})$ and time derivative of the wavenumber vector $\mathbf{k} = (k_x, k_z)$, which are represented by

$$\frac{d_g \mathbf{X}}{dt} \equiv \mathbf{C}_g \tag{24}$$

$$\frac{d_g \mathbf{k}}{dt} \equiv \frac{\partial \mathbf{k}}{\partial t} + \mathbf{C}_g \cdot \nabla \mathbf{k} = -\nabla \Omega \tag{25}$$

where $\mathbf{X} = (X, Z)$ is the position of a ray; and Ω is the dispersion relation of MRGs. When a varying zonal flow $\overline{u}(x, z)$ exists, Ω and $\mathbf{C}_g \equiv (\partial\Omega/\partial k_x, \partial\Omega/\partial k_z)$ are given by

$$\Omega \equiv \omega_i + k_x \overline{u} = \frac{c_e}{2}\left(k - \sqrt{k^2 + 4\beta/c_e}\right) + k_x \overline{u} \tag{26}$$

$$C_{gx} = \frac{c_e}{2}\left(1 - \frac{k_x}{\sqrt{k_x^2 + 4\beta/c_e}}\right) + \overline{u} \tag{27}$$

$$C_{gz} = \mp \frac{\omega_i^3}{N(k_x \omega_i + 2\beta)} \tag{28}$$

where ω_i is intrinsic frequency; $c_e = N/|k_z|$; and N is buoyancy frequency. Although the direction of the vertical phase propagation of MRGs can be both upward and downward, we assumed upward phase propagation (i.e., $k_z < 0$ for $k_x > 0$ and $\omega_i < 0$) because of the eastward-tilted vertical structure (Fig. S3b). Thus, the minus sign is taken in (27), which corresponds to the downward energy dispersion for $\omega_i < 0$. If initial k_x and k_z are given, we can obtain $\mathbf{C}_g$ uniquely using (26)–(28) and start the time integration of (24) and (25) from an arbitrary initial position $\mathbf{X}_{init}$. Subsequently, $\mathbf{k}$, $\mathbf{C}_g$, and $\mathbf{X}$ is updated in turn. We use the fourth-order Runge-Kutta scheme with a time step of 30

min. Background fields ($\overline{u}$ and N) are calculated by linear and spline interpolation of the 6-hourly ERA-Interim data (7.5°S–7.5°N) in space and time, respectively.

As described in the main text (Section 4.2), the initial ray position $\mathbf{X}_{init}$ is around 49°E, 300 hPa ($\sim$ 9680 m), and the initial zonal wavelength λ_x ($= 2\pi/k_x$) is set to be about 47° (see Figs. S3b and S4). Meanwhile, this estimation should include some uncertainties, so we prepare for 45 initial conditions with slight perturbations for $\mathbf{X}_{init}$ and λ_x. Specifically, we have tried combinations of 5 zonal positions (X_{init} = 48°, 48.5°, 49°, 49.5°, 50°), 3 vertical positions (Z_{init} = 9630, 9680, 9730 m), and 3 zonal wavelengths (λ_x = 46°, 47°, 48°). For each λ_x and $c_{px} = -17.0$ m/s (Fig. S4), k_z is determined by the MRG dispersion relation (26) as

$$|k_z| = N\frac{\beta/k_x^2 + c_{px}^i}{(c_{px}^i)^2} \tag{29}$$

where $c_{px}^i = \omega_i/k_x$ ($= c_{px} - \overline{u}$) is the intrinsic zonal phase speed. Consequently, initial λ_z is calculated as λ_z = 19.1, 21.4, and 25.8 km for λ_x = 46°, 47°, and 48°, respectively.

References

Aiyyer, A. R., & Molinari, J. (2003). Evolution of Mixed Rossby–Gravity Waves in Idealized MJO Environments. *J. Atmos. Sci.*, *60*(23), 2837–2855. doi: 10.1175/1520-0469(2003)060⟨2837:EOMRWI⟩2.0.CO;2

Haertel, P. T., & Kiladis, G. N. (2004). Dynamics of 2-Day Equatorial Waves. *J. Atmos. Sci.*, *61*(22), 2707–2721. doi: 10.1175/JAS3352.1

Kiladis, G. N., Wheeler, M. C., Haertel, P. T., Straub, K. H., & Roundy, P. E. (2009). Convectively coupled equatorial waves. *Rev. Geophys.*, *47*(2), RG2003. doi: 10.1029/2008RG000266

Majda, A. J. (2003). *Introduction to PDEs and waves in atmosphere and ocean* (1st ed.). Amer Mathematical Society.

Stechmann, S. N., Majda, A. J., & Khouider, B. (2008). Nonlinear dynamics of hydrostatic internal gravity waves. *Theor. Comput. Fluid Dyn.*, *22*, 407–432. doi: 10.1007/s00162-008-0080-7

Takayabu, Y. N., Lau, K.-M., & Sui, C.-H. (1996). Observation of a Quasi-2-Day Wave during TOGA COARE. *Mon. Wea. Rev.*, *124*(9), 1892–1913.

Yang, Q., Khouider, B., Majda, A. J., & Chevrotière, D. L. (2019). Northward Propagation, Initiation, and Termination of Boreal Summer Intraseasonal Oscillations in a Zonally Symmetric Model. *Journal of the Atmospheric Sciences*, *76*, 639–668. doi: 10.1175/JAS-D-18-0178.1

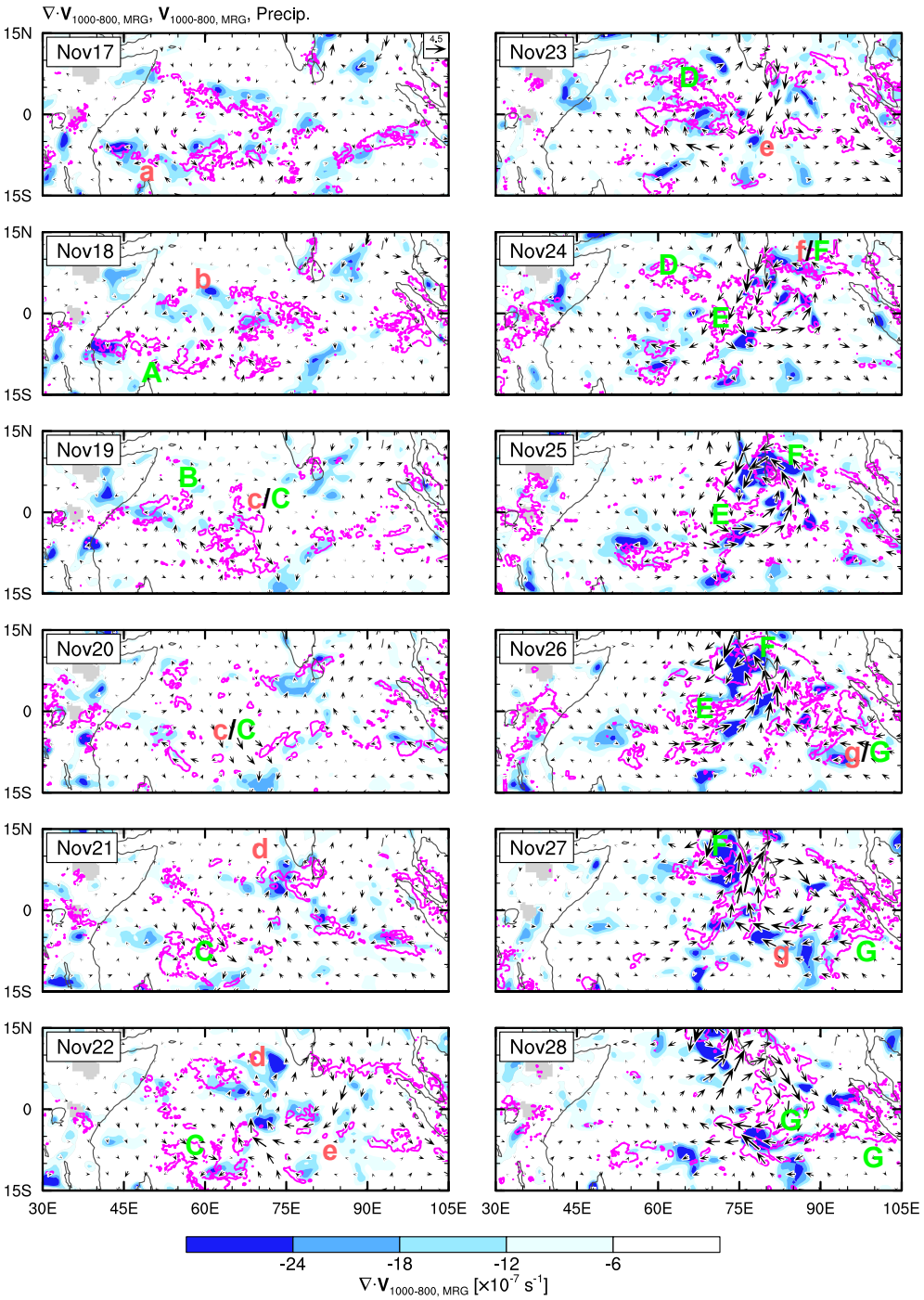

Figure S1. Horizontal maps of MRG-filtered horizontal convergence (shading) and wind anomalies (vectors) at 1000–800 hPa and precipitation (contours with 0.75 mm/hr) from 00UTC 17 to 28 November. Letters a–g and A–G′ denote representative convergence/cross-equatorial flows and corresponding precipitation, respectively (e.g., Convergence "a" is related to precipitation "A", associated with MJO initiation around 17 November).

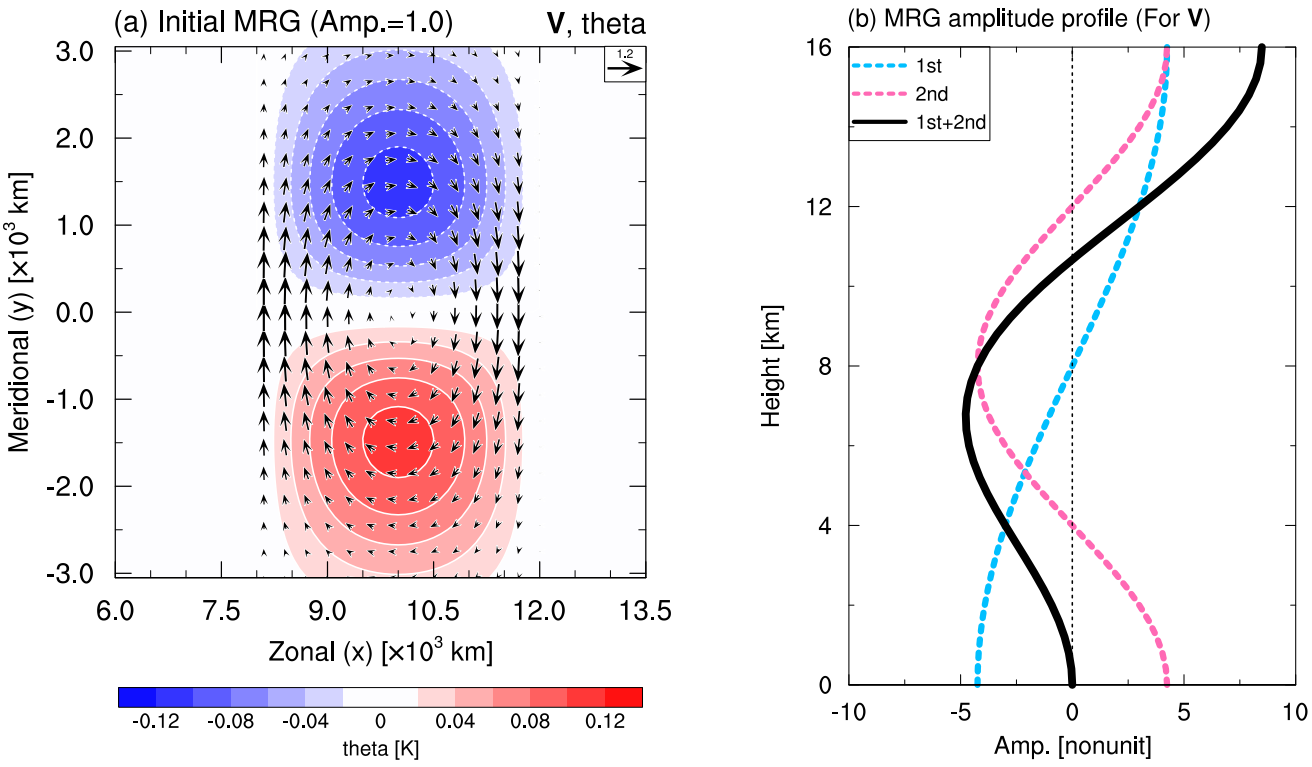

Figure S2. (a) Horizontal map of potential temperature (shading) and wind (vectors) anomalies given as the initial MRG structure for an MRG amplitude factor 1.0. (b) Vertical profile of an MRG amplitude factor for the first and second baroclinic modes (blue and pink) and their superposition (black).

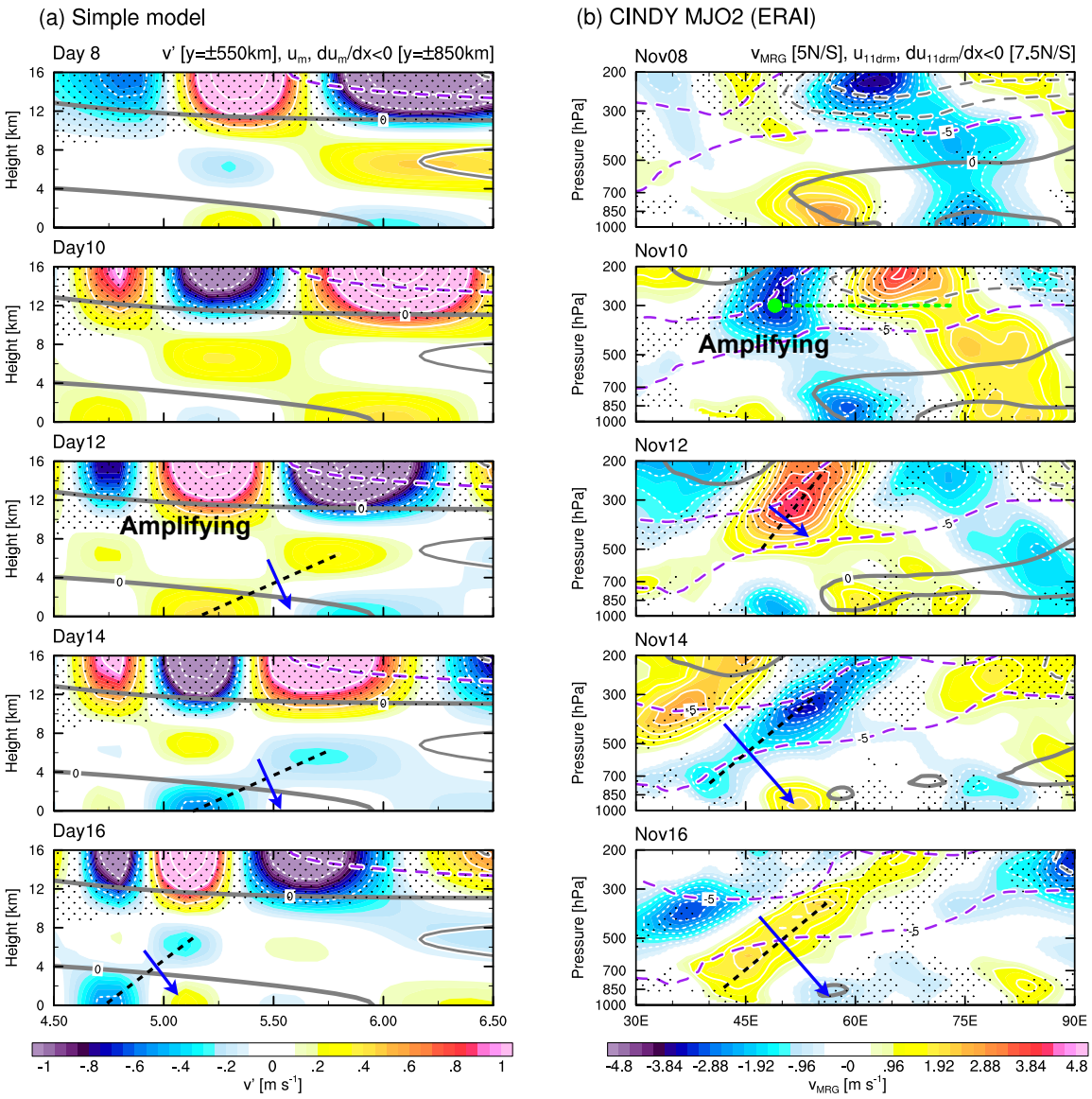

Figure S3. Zonal-height sections of equatorial MRG-related meridional wind anomalies (shading and white contours), background zonal winds (gray and purple contours), and background zonal convergence (stippling) every 2 day for (a) the model from days 8 to 16 and (b) MJO2 from 8 to 16 November. Definitions of anomalies and background fields follow those in Fig. 3. White contour interval is 0.5 (0.48) m/s for the model (MJO2). Gray/purple contour interval is 2.5 m/s from ±5 m/s (purple; −5 m/s), with negative (zero) values broken (bolded). Black-dashed lines and blue arrows represent the eastward-tilted phase lines and expected direction of MRG energy dispersion, respectively. Filled marker on 10 November in (b) denotes $\mathbf{X}_{init}$ for ray tracing.

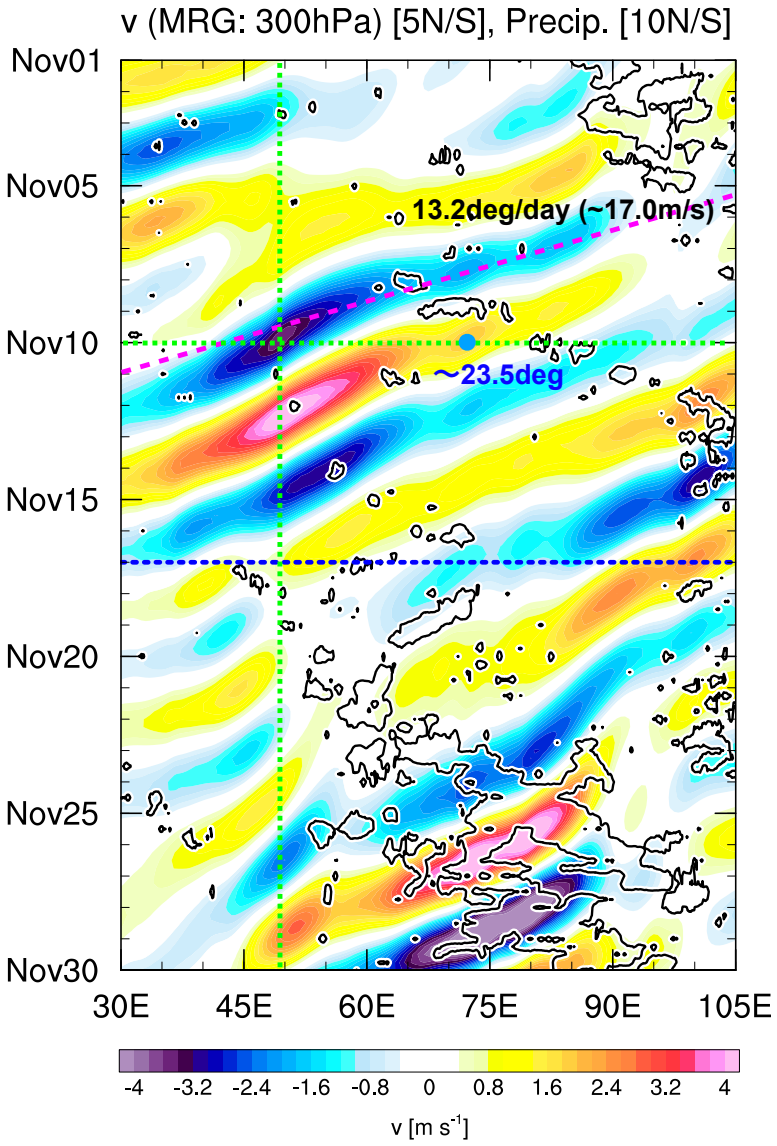

Figure S4. As in Fig. 1d, but for 300 hPa.